# De novo discovery of phenotypic intratumour heterogeneity using imaging mass spectrometry

Balluff, B.; Frese, C.K.; Maier, S.K.; Schone, C.; Kuster, B.; Schmitt, M.; ... ; McDonnell, L.A.

**Journal of Pathology**
*J Pathol* 2015; **235:** 3–13
Published online 3 November 2014 in Wiley Online Library (wileyonlinelibrary.com) DOI: 10.1002/path.4436

**ORIGINAL PAPER**

# *De novo* discovery of phenotypic intratumour heterogeneity using imaging mass spectrometry

Benjamin Balluff,[1] Christian K Frese,[2] Stefan K Maier,[3,4] Cédrik Schöne,[3] Bernhard Kuster,[4] Manfred Schmitt,[5] Michaela Aubele,[6] Heinz Höfler,[6,7] André M Deelder,[1] Albert JR Heck,[2] Pancras CW Hogendoorn,[8] Johannes Morreau,[8] AF Maarten Altelaar,[2] Axel Walch[3#] and Liam A McDonnell[1,9,#*]

[1] *Centre for Proteomics and Metabolomics, Leiden University Medical Centre, The Netherlands*
[2] *Biomolecular Mass Spectrometry and Proteomics Group, Bijvoet Centre for Biomolecular Research and Utrecht Institute for Pharmaceutical Sciences, Utrecht University, The Netherlands*
[3] *Research Unit Analytical Pathology, Helmholtz Zentrum München–German Research Centre for Environmental Health, Neuherberg, Germany*
[4] *Department of Proteomics and Bioanalytics, Technische Universität München, Freising, Germany*
[5] *Department of Obstetrics and Gynaecology, Klinikum Rechts der Isar, Technische Universität München, Germany*
[6] *Institute of Pathology, Helmholtz Zentrum München–German Research Centre for Environmental Health, Neuherberg, Germany*
[7] *Institute of Pathology, Klinikum Rechts der Isar, Technische Universität München, Germany*
[8] *Department of Pathology, Leiden University Medical Centre, The Netherlands*
[9] *Pisa Science Foundation, Italy*

**Correspondence to: LA McDonnell, Centre for Proteomics and Metabolomics, Leiden University Medical Centre, Einthovenweg 20, 2333 ZC Leiden, The Netherlands. E-mail: L.A.Mcdonnell@lumc.nl*

[#]These authors contributed equally to this study.

## Abstract

**An essential and so far unresolved factor influencing the evolution of cancer and the clinical management of patients is intratumour clonal and phenotypic heterogeneity. However, the *de novo* identification of tumour subpopulations is so far both a challenging and an unresolved task. Here we present the first systematic approach for the *de novo* discovery of clinically detrimental molecular tumour subpopulations. In this proof-of-principle study, spatially resolved, tumour-specific mass spectra were acquired, using matrix-assisted laser desorption/ionization (MALDI) imaging mass spectrometry, from tissues of 63 gastric carcinoma and 32 breast carcinoma patients. The mass spectra, representing the proteomic heterogeneity within tumour areas, were grouped by a corroborated statistical clustering algorithm in order to obtain segmentation maps of molecularly distinct regions. These regions were presumed to represent different phenotypic tumour subpopulations. This was confirmed by linking the presence of these tumour subpopulations to the patients' clinical data. This revealed several of the detected tumour subpopulations to be associated with a different overall survival of the gastric cancer patients ($p = 0.025$) and the presence of locoregional metastases in patients with breast cancer ($p = 0.036$). The procedure presented is generic and opens novel options in cancer research, as it reveals microscopically indistinct tumour subpopulations that have an adverse impact on clinical outcome. This enables their further molecular characterization for deeper insights into the biological processes of cancer, which may finally lead to new targeted therapies.**


**Keywords:** intratumour heterogeneity; proteomics; imaging mass spectrometry; metastasis; survival

Received 3 June 2014; Revised 4 August 2014; Accepted 3 September 2014

*No conflicts of interest were declared.*

## Introduction

Intratumour heterogeneity is an important factor influencing the evolution of cancer and the clinical management of patients [1–3]. It has been postulated to result from either clonal evolution, based on genetic instability and microenvironmental stresses, or multilineage differentiation of cancer stem cells [4,5]. Although these cancer cell populations can be histologically indistinguishable at the microscopical level [6], they are thought to have unique molecular phenotypes (here referred to as 'tumour subpopulations') that drive tumour progression and determine the disease outcome of the patient [7]. The identification of these clinically relevant tumour subpopulations is thus of utmost importance for understanding cancer development and the role of intratumour heterogeneity in the management of cancer patients [8].

While histological heterogeneity has long been known since the early days of cancer pathology, molecular tumour heterogeneity has mainly been described at a genetic, chromosomal or transcriptomal level [9]. For proteins, the clinical implications of tumour

heterogeneity have mainly been investigated by targeted assays using antibodies. This requires *a priori* knowledge of the protein to be studied and is therefore unsuited to discovery-based research of novel tumour subpopulations [10]. Hence, the *de novo* identification of tumour subpopulations with unequal proteomes requires an unlabelled and spatially resolved *in situ* read-out of the molecular information of the tumour.

An emerging technology that fulfils these requirements is matrix-assisted laser desorption/ionization (MALDI) imaging mass spectrometry ('MALDI imaging') [11,12]. It combines mass spectrometry with microscopy of tissues, which enables the unlabelled imaging of different molecular classes (proteins, peptides, lipids, metabolites) in their histological context and thus the allocation of molecular profiles to specific cell types, such as tumour, preneoplastic or inflammatory cells [13–15]. The spatially resolved data facilitate the investigation of intrasample molecular details, such as tumour/normal interface zones or intratumour heterogeneity [16,17]. In the latter, it has been convincingly demonstrated that MALDI imaging in combination with statistical tools constitutes a unique tool to reveal tumour subpopulations that are *a priori* not distinguishable by conventional histopathological methods, but which are molecularly distinct [16,18–20]. However, none of the hitherto performed studies has investigated which of the identified specific subpopulations drives the disease outcome in patients, such as locoregional and distant metastasis, or survival.

This study will show for the first time how MALDI imaging of tumour tissues in combination with advanced statistical clustering methods can be used to identify phenotypically and molecularly distinct tumour subpopulations with clinical relevance in breast and gastric cancer.

## Materials and methods

### Study population and tissues

All samples were fresh-frozen tissues stored in liquid nitrogen until measurement. They were obtained from patients who underwent primary surgical resection at the Klinikum Rechts der Isar, Munich, Germany. All gastric cancer patients were matched to the stage of their primary tumor (pT = 2) based on the cancer staging system of the Union for International Cancer Control (UICC), and to Lauren's classification (intestinal type). Follow-up data was available for all gastric cancer patients; median overall survival time was 33.1 (range 0–53.4) months. Breast cancer samples were all from invasive ductal carcinoma and patients with nodal metastases were matched to the amount of regional lymph nodes involved (UICC-pN = 1). This study was approved by the Institutional Review Board and the Ethics Committee of the Faculty of Medicine of the Technische Universität München, with informed consent from all subjects and patients. The clinicopathological data of both patient series are listed in Table 1.

Table 1. Clinicopathological parameters for the patient series

| | Gastric carcinoma | Breast carcinoma |
|---|---|---|
| Number of patients | 63 | 32 |
| Primary tumour extension | | |
| pT1 | 0 | 13 |
| pT2 | 63 | 13 |
| pT3 | 0 | 2 |
| pT4 | 0 | 4 |
| Regional lymph nodes metastasis | | |
| pN0 | 18 | 11 |
| pN1 | 24 | 21 |
| pN2 | 16 | 0 |
| pN3 | 5 | 0 |
| Resection status | | |
| R0 | 53 | 28 |
| R1 | 9 | 1 |
| Rx | 1 | 3 |
| Distant metastasis | | |
| M0 | 54 | 32 |
| M1 | 9 | 0 |
| MALDI imaging parameters | | |
| Resolution (µm) | 70 | 70 |
| Mass range (Da) | 2500–25 000 | 2000–25 000 |

### MALDI imaging experiments – *in situ* proteomic data from cancer tissues

MALDI imaging experiments were conducted as described previously [21]. The mass spectrometric data were acquired using an Ultraflex III MALDI–TOF/TOF instrument (Bruker Daltonics, Bremen, Germany) in positive linear mode, in which proteins were detected in the mass range as given in Table 1 and a lateral resolution of 70 µm. Following the MALDI imaging experiments, the tissue sections were stained with haematoxylin and eosin (H&E), scanned using a digital slide-scanning system (Mirax Desk, Carl Zeiss MicroImaging, Göttingen, Germany) and co-registered to the MALDI imaging results to align mass spectrometric data with the histological features of the tissue sections.

### Data preprocessing – selection of tumour-specific protein profiles

The alignment of mass spectral data and histology allows for a histology-guided extraction (virtual microdissection) of tumour cell-specific spectral data, which was done using FlexImaging software (Bruker Daltonics). This results in an XML file which contains a list of all mass spectra belonging to the user-defined region of interest. All subsequent data processing was performed using MATLAB R2011a, including the bioinformatics and image processing toolboxes (MathWorks, Natick, MA, USA).

The spectra referenced in the XML files were read into the MATLAB environment, where they underwent total ion count normalization and recalibration on common peaks, which were defined to be peaks present in at least 85% of all samples [22]. Peak picking was performed on the global basepeak mass spectrum after smoothing, resampling and baseline subtraction, and was performed

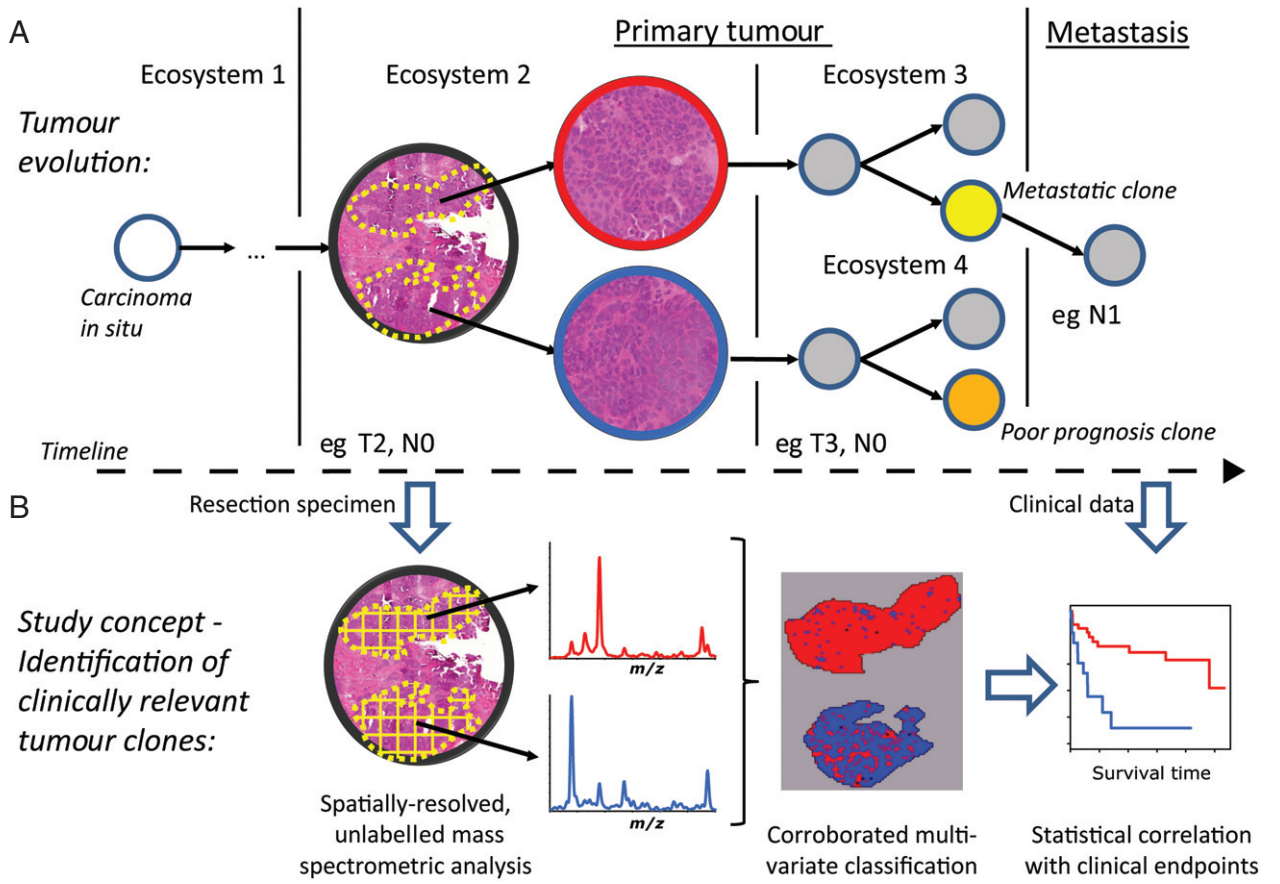


**Figure 1.** Methodological concept of this study. Intratumour clonal heterogeneity influences cancer evolution and the clinical outcome of patients (A). It is caused by micro-environmental selective stresses or multilineage differentiation of cancer stem cells, which can generate 'passenger' clones (grey circles), having no effect on the malignant development, or tumour 'driver' clones (coloured circles). The latter usually result in clinically measurable effects, such as tumour progression (clinical parameter T), metastasis (clinical parameter N) or follow-up data after surgery (eg survival time). (B) MALDI imaging mass spectrometry was used to obtain spatially resolved proteomic data (in the form of mass spectra) from primary tumour specimens. We hypothesize that statistical correlation of the patients' clinical data with the molecular diversity detected by a corroborated, unsupervised segmentation of the mass spectra can enable the identification of these tumour-driving subpopulations.

using an adapted version of the LIMPIC package [23]. The basepeak spectrum displays the maximum intensity detected in the entire imaging dataset for every peak and is more effective for detecting peaks with localized expressions [23].

Peak areas were extracted from all spectra and this reduced representation of a mass spectrum-reduction takes place by only considering the data of detected peaks- was then placed, based on its original coordinate information, as a pixel into a project-specific data cube. The project data cube contained the MALDI imaging data of all samples, in which spatial offsets were used to place every sample's data into the same spatial domain (Figure 2A), with the corresponding mass spectral data in the $z$ dimension.

## Unsupervised identification of heterogeneity

For *a priori* identification of intratumour biomolecular heterogeneity, we made use of the multivariate nature of MALDI imaging data (here simultaneous detection of many proteins). A number of multivariate statistical methods exist that enable the identification of regions with distinct protein signatures. However, these different algorithms optimize different functions; consequently their results can differ. We therefore developed a method for the corroborated identification of molecular heterogeneity, previously termed 'agreement analysis' [24], which consists of the independent application and subsequent combination of five multivariate data analysis (MVA) methods, including principal component analysis (PCA), maximum autocorrelation factorization (MAF), Fuzzy C-means, probabilistic latent semantic analysis (PLSA) and non-negative matrix factorization (NNMF). Each of these methods projects the original multivariate data into a new, usually reduced, data space, with new variables, called components, and transformed original values, called scores. While NNMF, PLSA and Fuzzy C-means require the user to predefine the number of expected components ($k$) – which here is considered equal to the number of expected tumour subpopulations – PCA and MAF do not require such a prior selection. Instead, the top $2 \times k$ components were selected and the negative and positive scores treated separately. The agreement analysis then works as follows.

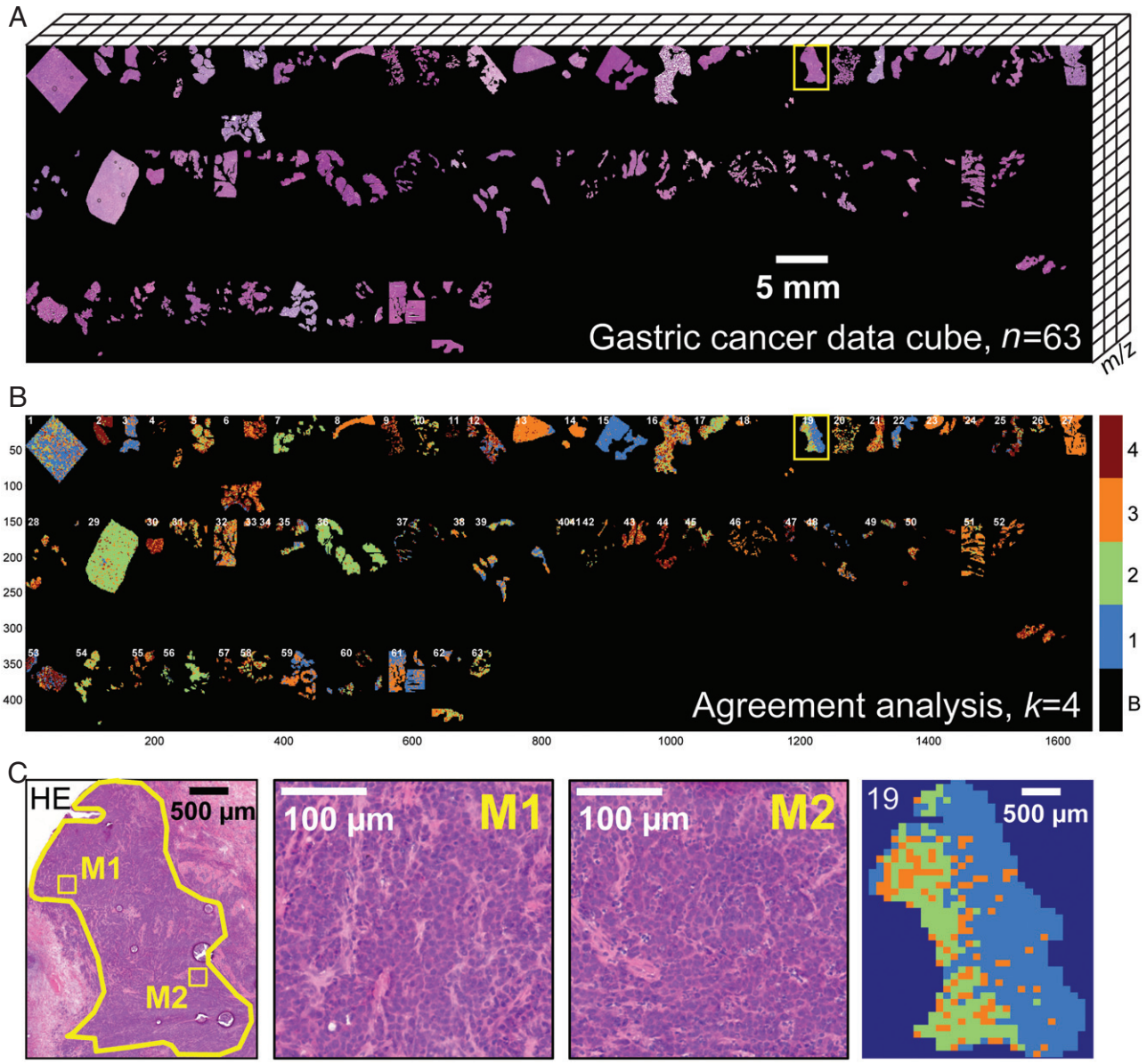


**Figure 2.** Intratumour heterogeneity in intestinal-type gastric cancer: 63 tissues were measured by MALDI imaging and the mass spectral data (*m/z*) of all samples were spatially arranged in the MATLAB environment (A). The agreement analysis was performed for different *k* values (2–10), which revealed substantial tumour heterogeneity, as shown in the segmentation image for $k = 4$ (B). Higher-magnification images of patient 19 demonstrate the histomorphological homogeneity within the measured tumour area (left panels), despite its clear molecular heterogeneity, represented by clusters 1 and 2 (far right panel) (C).

After defining *k*, all components returned by the MVA methods are compared pairwise by calculating the Pearson correlation coefficient. Components that show the highest spatial correlation were then normalized to their maximum score and summed by a per-pixel score addition. In this way, consensus components are obtained. The degree of agreement of a consensus component is indicated by the sum of the correlation coefficients between the five multivariate methods, and hence is in the range 0–4. In this study, consensus components with a score<1 were excluded from further analyses. It is important to note that more than *k* consensus components may be returned if correlated components are found by a subset of the MVA methods.

Finally, a segmentation image is achieved by assigning each pixel to the consensus component with the highest score at that location. This image shows molecularly different regions (clusters) in different colours. In this manner tumour subpopulations, represented by clusters with distinct and robust mass spectral profiles, could be identified.

## Statistical analysis – comparison with clinical endpoints

The statistical analysis required linking the clinical data of the samples to the presence of specific clusters (tumour subpopulations) within a sample. To do so, a sample was assigned to a cluster if the cluster was

sufficiently present in that sample; formalized, if the cluster held a higher fraction of pixels than would be possible by chance alone, i.e. $\geq 1/k \times 100\%$ pixels. A single patient sample may be assigned to more than one cluster if it contains significant tumour heterogeneity. Conversely, each cluster could be linked to the clinical data of the multiple samples associated with it, which then allowed comparison of each cluster's clinical importance. The clinical data can also be used to retrospectively investigate the pixel fraction threshold, eg to elucidate the minimum presence of a cluster to affect the patients' clinical outcome, as described in Protocol S2 (see supplementary material).

The statistical comparisons between the clusters' clinical data were performed within the R statistical environment (R Foundation for Statistical Computing, Vienna, Austria), in which $p<0.05$ was considered statistically significant. Differences in survival times of the clusters were assessed by Kaplan–Meier analysis and the log-rank test. Multivariate survival analyses to assess the independent prognostic value of the clusters were done by Cox regression, with $p$ values calculated by the Wald test. Correlations of the clusters with metastatic status were assessed by Fisher's exact test.

The phylogenetic reconstruction of the protein signals distinguishing tumour subpopulations was performed in MATLAB, using the neighbour-joining algorithm with Euclidean distance metric between the representative spectra of the clusters. In order to avoid a bias towards the most intense peaks, the representative spectra of each cluster were normalized according to their base peak. The most discriminative mass signal for a branching point with respect to its child nodes was determined by comparing the representative spectra of both child nodes for the highest-intensity difference. The representative spectrum of each inner node was iteratively calculated by averaging the spectra of all clusters that are leaf nodes of that node.

### Protein identification

Direct tissue analysis using MALDI imaging detects intact proteins as well as protein fragments. In a first step, peaks of interest highlighted by the statistical analysis were compared with those previously reported in the literature and summarized in two recently reported MALDI imaging identification databases [25,26]. This was followed by extensive LC–MS/MS characterization of tissue extracts using top-down tandem mass spectrometry, using HCD and ETD on an Orbitrap Elite mass spectrometer coupled to a Proxeon EASY-nLC 1000 system. Detailed information can be found in Protocol S1 (see supplementary material).

## Results

The central hypotheses of this study were: (a) the primary tumour consisted of a collection of subpopulations that reflected the evolution of the tumour, in which the presence of subpopulations with specific characteristics could ultimately lead to increased proliferation, metastasis or resistance to chemo- or radiotherapy (Figure 1A); (b) the molecular intratumour heterogeneity revealed by MALDI imaging depicted, however incompletely, a representation of these tumour subpopulations. We then used the clinical data of the patients to identify which subpopulations were associated with specific phenotypes (Figure 1B). In this section, we provide examples in two different cancer types, namely breast and gastric cancer, for the capability of the approach presented here to identify tumour subpopulations that are associated with the disease outcome of patients.

### Identification of survival-associated tumour subpopulations in primary gastric cancer

First, we applied our approach to identify tumour subpopulations associated with prognosis in intestinal-type gastric cancer. Tissue sections from 63 patients were measured by MALDI imaging with a lateral resolution of 70 µm to detect mass spectral profiles. After the experiments, the tissues were stained with H&E and histopathologically annotated. Virtual microdissection was then performed to obtain spatially resolved mass spectra from histologically uniform tumour areas. The resulting 54 833 mass spectra were arranged in a project-specific data cube (Figure 2A) and segmented using the agreement analysis on the 82 detected mass spectral signals to reveal molecularly distinct subpopulations within the tumour areas.

As the number of subpopulations present in a tumour is unknown, the molecular segmentation was run with different values for the number of expected tumour subpopulations ($k$), in the range 2–10. It should be noted that the clustering was performed simultaneously on all samples, as it was assumed that phenotypically important tumour subpopulations would display similar molecular characteristics in all patient samples. For instance, the results for $k=4$ in Figure 2B show that the agreement analysis was able to reveal molecularly distinct regions within histomorphologically homogeneous tumour areas in about one-third of the 63 samples. One example at higher magnification is shown in Figure 2C.

In order to determine the clinical importance of each tumour subpopulation, the results of the molecular segmentation had to be linked to the clinical data of the patients. A tumour subpopulation was associated with the clinical data of a patient if it contributed more pixels to that sample than would be found by chance alone; eg sample 19 in Figure 2C contained tumour subpopulations numbers 1 and 2, as each of them held >25% (for $k=4$) of the pixels of that sample.

The tumour subpopulations could then be statistically compared according to their associated clinical data; here, for the difference in their overall survival. Statistically significant differences in overall survival were found for $k=6$ and $k=9$ between tumour subpopulations 1 versus 4 ($p=0.025$) and 1 versus 7 ($p=0.044$), respectively. Moreover, the presence of

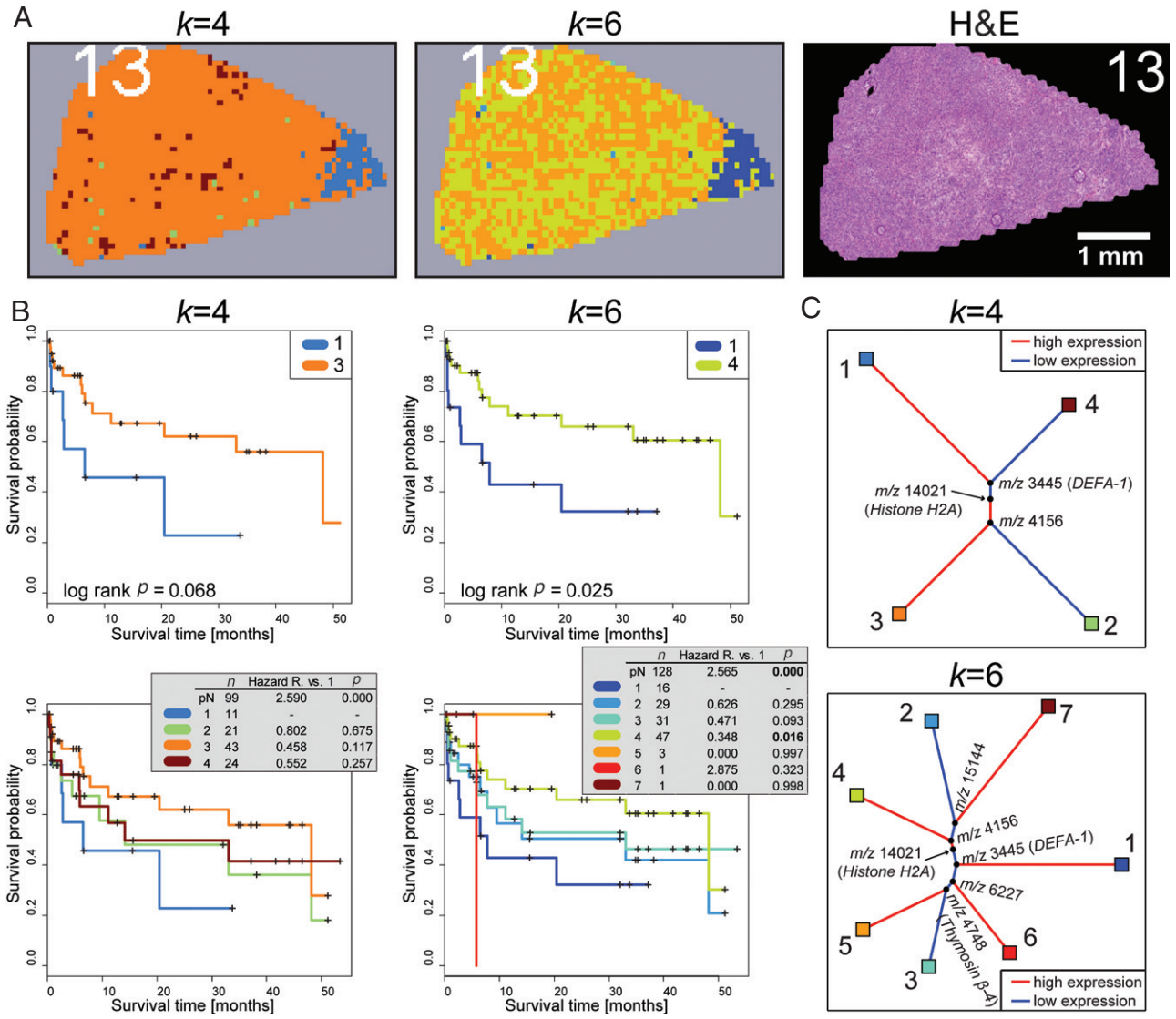


**Figure 3.** Assessment of clinical relevance of the identified tumour subpopulations according to their associated clinical data. Kaplan–Meier analysis revealed that the presence of certain tumour subpopulations (clusters) is indicative of overall survival in gastric cancer patients (B). While the survival difference between clusters 1 and 3 for $k = 4$ was close to significant, the difference between the topologically same clusters 1 and 4 for $k = 6$ was significant (B, upper panel). Moreover, these clusters turned out to be independent prognostic factors compared to the metastatic status (pN) (B, lower panel). The topological (A) and clinical consistency of these tumour subpopulations indicates their robustness towards a changing $k$, which is further examined in Figure 4. Phylogenetic analyses show the relationship between all clusters, which are represented by leaf nodes (C). Internal nodes indicate the most decisive *m/z* signal between two child nodes. Here, three signals, *m/z* 3445 (DEFA-1), 4156 and 14021 (histone H2A), were consistently found to be major contributors for distinguishing good from poor survivor subpopulations.

these tumour subpopulations in a sample was predictive of survival independently of regional lymph node metastases (Figure 3B; see also supplementary material, Table S1). Good and poor survivor groups at trend level could also be observed when $k$ was defined as 4, 7 or 8, between clusters 1 versus 3 ($p = 0.068$), 1 versus 6 ($p = 0.068$) and 1 versus 5 ($p = 0.058$), respectively. Figure 3B, C depicts the Kaplan–Meier graphs for $k = 4$ and $k = 6$ and the corresponding phylogenetic reconstruction between the clusters. The latter summarizes the molecular relationship between the tumour subpopulations and highlights the most discriminating mass signals at each branching node. Tumour subpopulations indicative of poor and good survival were consistently found ($k = 4$ and $k = 6$) to be characterized by higher levels of *m/z* 3445 and 4156, and a significant change in *m/z* 14 021 (Figure 3C); *m/z* 3445 and 14021 could be identified as DEFA-1 and histone H2A, respectively (see supplementary material, Protocol S1).

Figure 3 also shows that a significant prognostic effect only became visible after increasing $k$ to differentiate smaller tumour subpopulations. An example of such a subdivision of a tumour population into two finer subpopulations is illustrated in Figure 3A. To further study the effect of the refinement of tumour populations on their clinical phenotypes, the survival analysis was performed on all subpopulations detected for $k = 2–10$. A dendrogram-like overview illustrates the results for

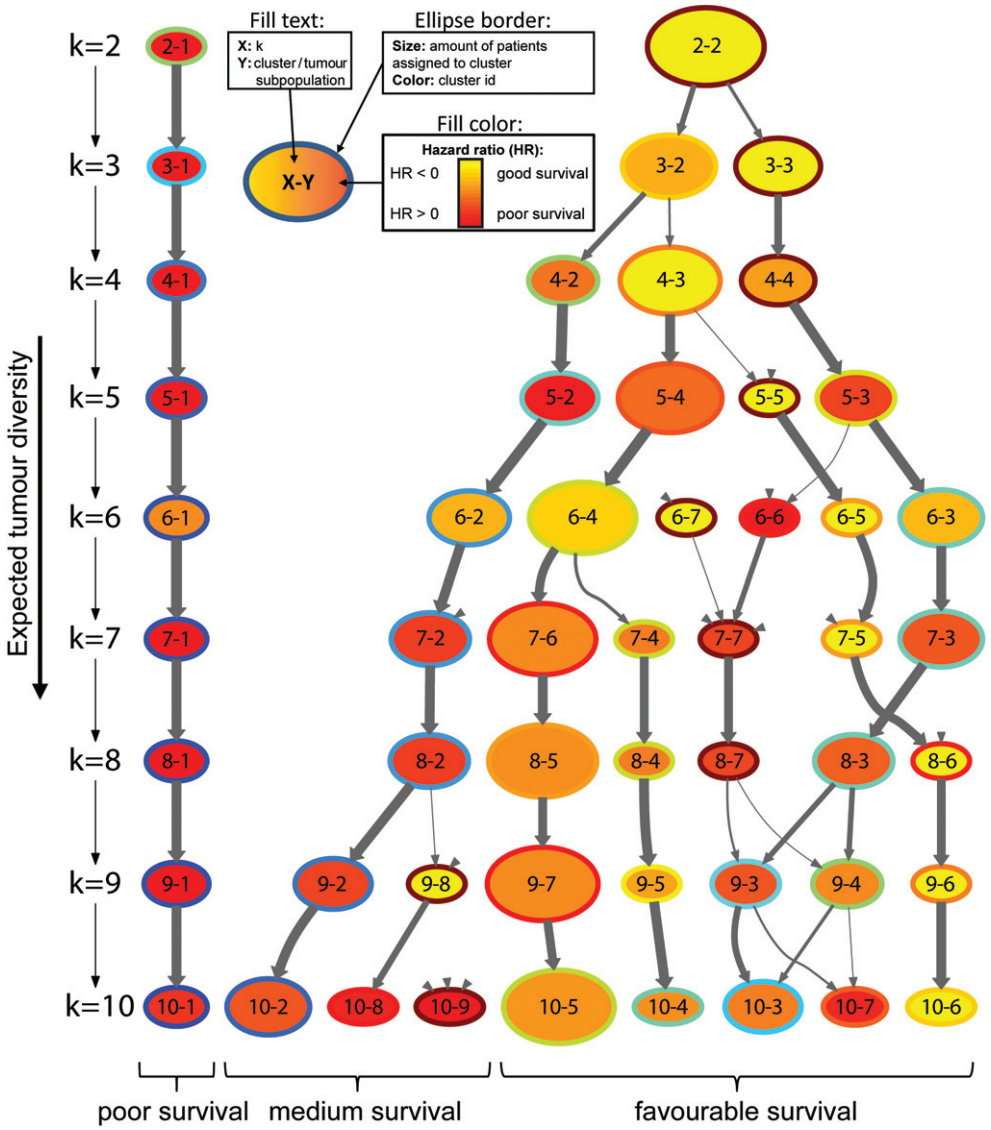


**Figure 4.** Graph-based analysis for the assessment of tumour diversity and its prognostic value in gastric cancer. Ellipses represent tumour subpopulations (clusters), which can be identified through their ID (nomenclature: first digit = *k*, second digit = cluster) or border colour. The size of an ellipse is proportional to its incidence among patients and its survival hazard ratio is colour-coded as fill colour (both were normalized level-wise). The vertical dimension shows the effect of a changing *k*, the parameter that controls the number of tumour subpopulations expected, which leads to subdivisions of existing clusters into new clusters. The strength of topological correlation (0–1) between clusters in consecutive segmentation images is represented by the thickness of arrows between ellipses. Clusters that are less split into new clusters by increasing *k* are considered molecularly robust, such as cluster 1. It can also be observed that, although an increasing *k* leads to an increasing diversification, three main groups with different survival behaviour could be observed, which can be traced back to the levels $k = 3–4$.

each detected tumour subpopulation, i.e. its clinical importance in terms of prognostic value and its incidence amongst patients, and its parent tumour subpopulations (Figure 4). The parent subpopulation is defined as the one that has the highest spatial congruence in the previous segmentation map ($k - 1$). Therefore, correlation coefficients between consecutive segmentation maps were calculated (to identify related clusters, only positive correlations were considered), which are represented as arrows between the tumour subpopulations in Figure 4. Consequently, parent tumour subpopulations are considered molecularly robust if they are insensitive to being subdivided in a subsequent *k*. In this case, tracing the correlations from $k = 10$ backwards shows that several tumour subpopulations (clusters 1, 2, 4, 5 and 6 of $k = 10$ in Figure 4) exhibit a high robustness across the different levels, including those with poor and good overall survival. With an increasing number of expected clusters (*k*), a steady diversification could be observed, finally revealing three major groupings of tumour subpopulations associated with a poor, medium and good survival, which can be traced back to the levels $k = 3/4$ (Figure 4).

To test the general applicability of the technique, we then tested whether the approach of using clinical endpoints to identify tumour driver subpopulations – here demonstrated for patient survival – could also be applied to detect those associated with metastasis, which

is a strong determinant for patient disease outcome and also thought to derive from clonal diversity.

### Metastasis-associated subpopulations in primary breast cancer

Tissue sections from 32 breast cancer patients were measured by MALDI imaging with a lateral resolution of 70 µm. Proteomic data from histologically uniform areas was obtained via virtual microdissection and arranged in a project-specific data cube (Figure 5A). Of the 32 patients, 21 showed lymph node metastasis (pN1) and 11 were metastasis-free (pN0). To investigate associations between subpopulations in the primary tumours and their metastatic status, the 48 426 tumour-specific mass spectra (mass range, *m/z* 2000–25 000; 62 protein signals) were submitted to agreement analysis, with $k$ in the range 2–10.

The classification image in Figure 5B displays the result of the agreement analysis for $k = 5$. The analysis revealed molecularly distinct regions within histologically homogeneous tumour areas. For example, the tumour area of patient 22 was found to be mainly composed of the molecularly distinct subpopulations 1 and 4 (Figure 5C). A statistically significant association ($p = 0.036$) was found between tumour subpopulation 4 and the metastatic samples (pN1; bar plot in Figure 5D). This tumour subpopulation was topologically robust and consistently associated with metastatic samples, as indicated by the graph-based analysis from $k = 5$ onwards (see supplementary material, Figure S1). The molecular characteristics of this tumour subpopulation were assessed by phylogenetic analysis (Figure 5D), which revealed that it was characterized by the presence of *m/z* 11368 and an absence of *m/z* 8419 and 14021; *m/z* 11368 and 14021 could be identified as acetylated histone H4 and histone H2A, respectively (see supplementary material, Protocol S1).

## Discussion

The *de novo* identification of phenotypic tumour subpopulations in patient tissue and their molecular features is both a challenging and an unresolved task. In this proof-of-concept study we linked the clinical information of patients to the molecularly distinct regions detected by MALDI imaging (in this paper referred to as 'tumour subpopulations'). This was done under the assumption that a tumour resection specimen – constituting a snapshot of intratumour heterogeneity at a certain time point of tumour progression – may still contain molecular information indicative of the subsequent disease outcome of the patient (Figure 1).

The analysis of 63 intestinal-type gastric cancer patients revealed extensive heterogeneity within and between individual tumour samples (Figure 2). Linking this heterogeneity to the clinical data revealed several of the regions to be associated with a different and independent overall survival, and thus a different disease outcome for the patients (Figure 3). Especially tumour subpopulation 1 (any $k$) indicated a significantly unfavourable prognosis for the patient. Moreover, a proteomic similarity of this 'malicious' tumour subpopulation with a lymph node metastasis could be observed in one sample (see supplementary material, Figure S2).

The general applicability of this multi-factorial approach was confirmed by analysing another independent sample cohort for a different clinical endpoint; 32 primary breast cancer tissues were investigated for tumour subpopulations associated with the presence of regional lymph node metastasis. In comparison to the gastric cancer cohort, the breast cancer dataset exhibited less molecular heterogeneity. This is in line with previous reports that gastric cancer is a more heterogeneous disease than breast cancer [27–29]. In breast cancer it is important to differentiate the tumours by their molecular subtype (luminal, basal and Her2-positive), as these can strongly influence prognosis or metastasis [30]. As our sample cohort was mainly (90%) composed of luminal type (oestrogen receptor-positive) breast cancers, no correlation could be found between a cluster and a certain subtype (see supplementary material, Table S3). Still, one subpopulation was found to be significantly associated with the metastatic status of the patients. This is in concordance with the hypothesis that clones with metastatic potential are already present in the primary tumour [7].

The minimum amount of tumour subpopulation that is necessary to affect the clinical outcome of the patients was then investigated by optimizing the pixel contribution threshold to be associated with the clinical data, as described in Protocol S2 (see supplementary material). The results show that optimized thresholds can increase the statistical sensitivity between the presence of clusters and the clinical endpoints, and that significant effects were already detectable at thresholds of 10–14% in both cancer datasets. However, since single tissue sections are unlikely to represent the real proportions of the tumour subpopulations with respect to the entire tumour, these numbers have to be considered project-specific, and are thus not generalizable.

Another important parameter is the number of expected tumour subpopulations, $k$. As this number is *a priori* unknown [31], we propose a clinicobiological solution inspired by the trunk–branch model of intratumour heterogeneity [32]. Instead of seeking an optimal $k$, our graph-based solution looks at the changes of the decomposition over a varying $k$ (Figure 4; see also supplementary material, Figure S1), which enables the diversification in relationship with the clinical data to be investigated. In gastric cancer a high molecular diversity was found, in which clusters could be constantly subdivided into new robust subclusters (eg cluster 4 of $k = 6$ into clusters 4 and 6 of $k = 7$ in Figure 4). However, the clinical implications were less complex, as overall three survivor groups could be distinguished (poor, medium and good survival). This reflects the fact that

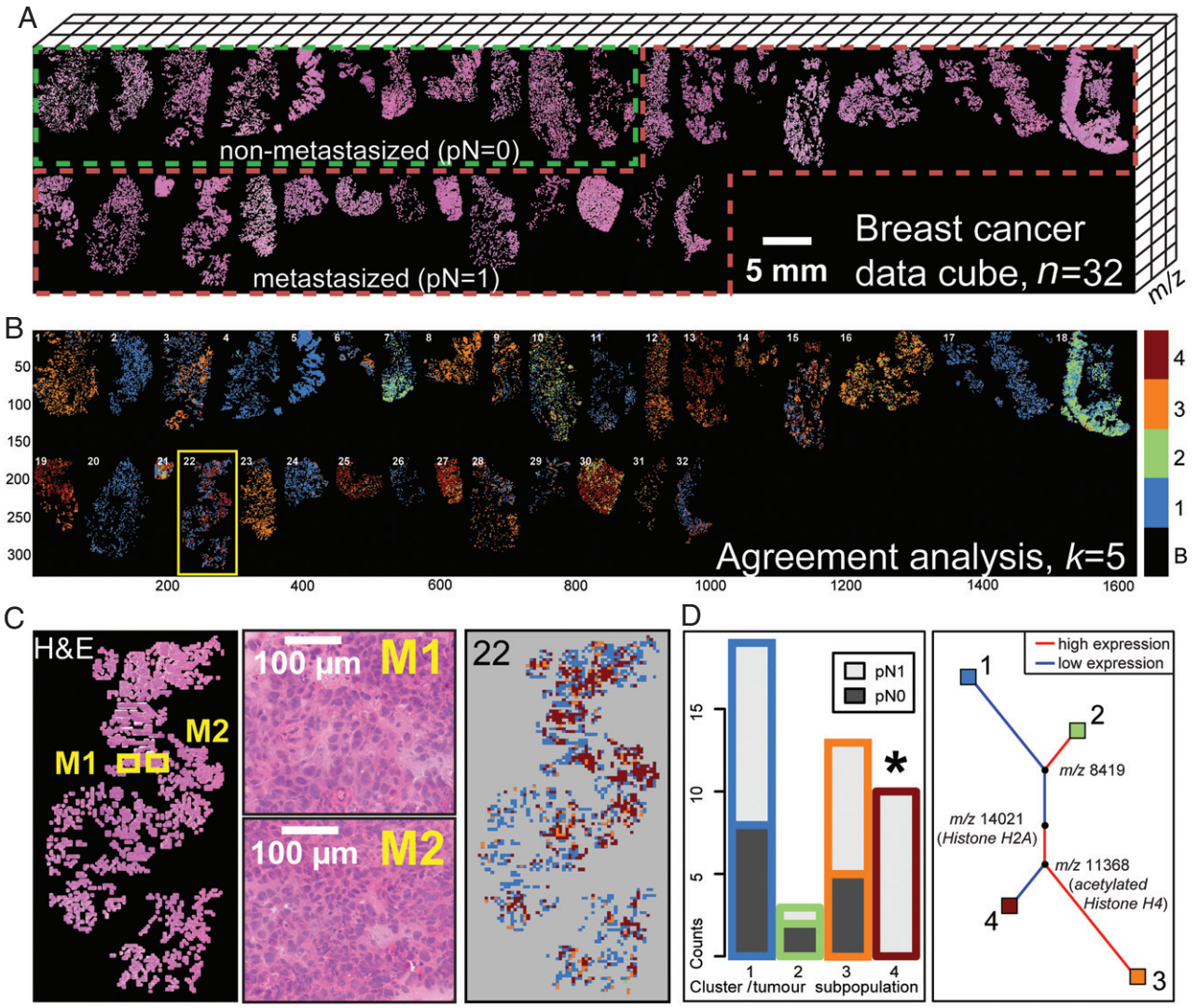


**Figure 5.** Tumour heterogeneity and metastatic status in 32 breast cancer samples. MALDI imaging mass spectral data (*m/z*) from histologically uniform regions of 21 metastasized and 11 non-metastasized breast cancer tissues was obtained (A). Agreement analysis was performed for different *k* values (2–10) and the results for $k = 5$ are shown (B). A higher-magnification example for patient 22 proves the histological homogeneity within the measured tumour area, despite the detected molecular heterogeneity represented by tumour subpopulations 1 and 4 (C). (D) Tumour subpopulation 4 was found to be significantly correlated with the metastatic status of the patients ($p = 0.036$) (bar plot) and characterized by changes in *m/z* 11368 (acetylated histone H4), 8419 and 14021 (histone H2A) (phylogenetic plot).

not every subpopulation will affect the disease's course. Additionally, it is likely that the available clinical data and number of samples were not able to fully resolve the molecular complexity in terms of prognostic effects (eg clusters 5 and 6 of $k = 6$ in Figure 3B). The analysis of a larger patient series and extended clinical follow-up are expected to lead to the detection of additional clinically relevant tumour subpopulations.

It is important to note that we have not yet established whether the tumour subpopulations detected by MALDI imaging represent different tumour clones that can be distinguished by mutations or other heritable properties. Instead, we take advantage of the fact that cellular selection operates on phenotypes [33] by measuring phenotypic information in form of mass spectral protein profiles. It should be noted that these phenotypic subpopulations were identified across the whole sample cohort, which implies that the proteomic patterns specific to these cell populations occurred in many tumour samples. This in turn suggests that these are likely general proteomic adaptations.

Phylogenetic analysis in both studies highlighted five major contributors to the proteomic pattern of the clinically most important tumour subpopulations: *m/z* 3445 (DEFA-1), 4156, 8416 and 11368 (acetylated histone H4) and 14021 (histone H2A) (Figures 3C, 5D; see also supplementary material, Protocol S1). All of them have already been detected in various cancer-focused MALDI imaging studies [34,35]. In particular, DEFA-1, which is an antimicrobial peptide expressed by neutrophils and also found in gastric cancer cells [36,37], was already reported to correlate with a poor prognosis of early-stage gastric cancer patients, hence confirming our results here [38,39]; *m/z* 4156 and 8416 could not be

named. Interestingly, *m/z* 4156 has only been detected in two other MALDI imaging studies on oesophageal adenocarcinoma, reporting its role in carcinogenesis and drug resistance [40,41]. However a prognostic value has not yet been found, not even in our previous study on the identification of prognostic markers in gastric cancer [38]. This omission was not due to the different data analysis platforms (ClinProTools versus MATLAB; see supplementary material, Figure S3), but rather due to the variable proportion of the phenotypic subpopulations in the different patient tissues.

The small number of cells analysed in each pixel, coupled with the absence of explicit protein purification or separation steps when MALDI is directly applied to tissue sections, means that MALDI imaging mainly detects abundant proteins [25]. Nonetheless, many studies using MALDI imaging and recently also a multicentre validation gave evidence for the robustness and meaningfulness of such protein signatures for representing clinically relevant information [42]. From our results we conclude that patterns of these abundant molecules constitute robust surrogate signals for different biochemical processes, which enable a separation of phenotypic tumour subpopulations with indistinguishable histology. In a next step, these regions can be microdissected and analysed using more sensitive, extraction-based approaches, such as high-throughput nucleic acid sequencing and state-of-the-art MS-based proteomics, which can delve deeply into the proteome and metabolome, as shown by Mann and coworkers [43]. In this way we expect to gain deeper insights into the underlying biological processes and changes of the tumour subpopulations on a genetic, metabolic and proteomic level, which might finally result in novel targeted therapies. Accordingly, we propose the approach presented here as the first step in a pipeline for the *de novo* identification and characterization of phenotypic tumour subpopulations, which we think is applicable to any kind of cancer tissue that exhibits substantial heterogeneity.

## Acknowledgements

We thank Dr Yuri EM van der Burgt and Simone Nicolardi for the MALDI–FTICR measurements (Centre for Proteomics and Metabolomics, Leiden University Medical Centre). This study was supported by the ZonMW Zenith project, Imaging Mass Spectrometry-based Molecular Histology: Differentiation and Characterization of Clinically Challenging Soft Tissue Sarcomas (Grant No. 93512002). BB was funded by the Marie Curie Action of the European Union (Grant No. SITH FP7-PEOPLE-2012–IEF 331866). AW was supported by the Ministry of Education and Research of the Federal Republic of Germany (BMBF; Grant Nos 0315505A, 01IB10004E and SYS-STOMACH) and the Deutsche Forschungsgemeinschaft (Grant Nos SFB 824 TP Z02 and WA 1656/3-1). MS and MA were supported by the Wilhelm Sander-Stiftung (Grant No. 2012.028.1).

## Author contributions

BB developed the method presented; BB, AW and LAM conceived and supervised the project and wrote the manuscript; CKF, SKM, BK, AJRH and AFMA were responsible for the protein identification; HH, MS and MA provided the samples and assisted in interpretation of the results; CS and BB were responsible for the MALDI imaging mass spectrometry data acquisition; AW and JM assisted in histological interpretation of the samples; AMD and PCWH assisted in interpretation of the results and writing the manuscript; and all authors approved the final version of the manuscript.

## References

1. Dalerba P, Kalisky T, Sahoo D, *et al.* Single-cell dissection of transcriptional heterogeneity in human colon tumors. *Nat Biotechnol* 2011; **29:** 1120–1127.
2. Gerlinger M, Rowan AJ, Horswell S, *et al.* Intratumor heterogeneity and branched evolution revealed by multiregion sequencing. *N Engl J Med* 2012; **366:** 883–892.
3. Maley CC, Galipeau PC, Finley JC, *et al.* Genetic clonal diversity predicts progression to esophageal adenocarcinoma. *Nat Genet* 2006; **38:** 468–473.
4. Marusyk A, Almendro V, Polyak K. Intra-tumour heterogeneity: a looking glass for cancer? *Nat Rev Cancer* 2012; **12:** 323–334.
5. Shibata D. Clonal diversity in tumor progression. *Nat Genet* 2006; **38:** 402–403.
6. Wu JM, Halushka MK, Argani P. Intratumoral heterogeneity of *HER-2* gene amplification and protein overexpression in breast cancer. *Hum Pathol* 2010; **41:** 914–917.
7. Greaves M, Maley CC. Clonal evolution in cancer. *Nature* 2012; **481:** 306–313.
8. Turner NC, Reis-Filho JS. Genetic heterogeneity and cancer drug resistance. *Lancet Oncol* 2012; **13:** e178–185.
9. Swanton C. Intratumor heterogeneity: evolution through space and time. *Cancer Res* 2012; **72:** 4875–4882.
10. Moeder CB, Giltnane JM, Harigopal M, *et al.* Quantitative justification of the change from 10% to 30% for human epidermal growth factor receptor 2 scoring in the American Society of Clinical Oncology/College of American Pathologists guidelines: tumor heterogeneity in breast cancer and its implications for tissue microarray based assessment of outcome. *J Clin Oncol* 2007; **25:** 5418–5425.
11. Norris JL, Caprioli RM. Analysis of tissue specimens by matrix-assisted laser desorption/ionization imaging mass spectrometry in biological and clinical research. *Chem Rev* 2013; **113:** 2309–2342.
12. Walch A, Rauser S, Deininger SO, *et al.* MALDI imaging mass spectrometry for direct tissue analysis: a new frontier for molecular histology. *Histochem Cell Biol* 2008; **130:** 421–434.
13. Balluff B, Rauser S, Ebert MP, *et al.* Direct molecular tissue analysis by MALDI imaging mass spectrometry in the field of gastrointestinal disease. *Gastroenterology* 2012; **143:** 544–549, e541–542.
14. McDonnell LA, Corthals GL, Willems SM, *et al.* Peptide and protein imaging mass spectrometry in cancer research. *J Proteomics* 2010; **73:** 1921–1944.
15. Schwamborn K, Caprioli RM. Molecular imaging by mass spectrometry – looking beyond classical histology. *Nat Rev Cancer* 2010; **10:** 639–646.
16. Deininger SO, Ebert MP, Futterer A, *et al.* MALDI imaging combined with hierarchical clustering as a new tool for the interpretation of complex human cancers. *J Proteome Res* 2008; **7:** 5230–5236.

17. Oppenheimer SR, Mi D, Sanders ME, *et al.* Molecular analysis of tumor margins by MALDI mass spectrometry in renal carcinoma. *J Proteome Res* 2010; **9:** 2182–2190.
18. Jones EA, Schmitz N, Waaijer CJ, *et al.* Imaging mass spectrometry-based molecular histology differentiates microscopically identical and heterogeneous tumors. *J Proteome Res* 2013; **12:** 1847–1855.
19. Turtoi A, Blomme A, Debois D, *et al.* Organized proteomic heterogeneity in colorectal cancer liver metastases and implications for therapies. *Hepatology* 2014; **59:** 924–934.
20. Willems SM, van Remoortere A, van Zeijl R, *et al.* Imaging mass spectrometry of myxoid sarcomas identifies proteins and lipids specific to tumour type and grade, and reveals biochemical intratumour heterogeneity. *J Pathol* 2010; **222:** 400–409.
21. Meding S, Walch A. MALDI imaging mass spectrometry for direct tissue analysis. *Methods Mol Biol* 2013; **931:** 537–546.
22. Norris JL, Cornett DS, Mobley JA, *et al.* Processing MALDI mass spectra to improve mass spectral direct tissue analysis. *Int J Mass Spectrom* 2007; **260:** 212–221.
23. McDonnell LA, van Remoortere A, de Velde N, *et al.* Imaging mass spectrometry data reduction: automated feature identification and extraction. *J Am Soc Mass Spectrom* 2010; **21:** 1969–1978.
24. Jones EA, van Remoortere A, van Zeijl RJ, *et al.* Multiple statistical analysis techniques corroborate intratumor heterogeneity in imaging mass spectrometry datasets of myxofibrosarcoma. *PLoS One* 2011; **6:** e24913.
25. Maier SK, Hahne H, Gholami AM, *et al.* Comprehensive identification of proteins from MALDI imaging. *Mol Cell Proteomics* 2013; **12:** 2901–2910.
26. McDonnell LA, Walch A, Stoeckli M, *et al.* MSiMass list: a public database of identifications for protein MALDI MS imaging. *J Proteome Res* 2014; **13:** 1138–1142.
27. Nadauld LD, Ford JM. Molecular profiling of gastric cancer: toward personalized cancer medicine. *J Clin Oncol* 2013; **31:** 838–839.
28. Lawrence MS, Stojanov P, Polak P, *et al.* Mutational heterogeneity in cancer and the search for new cancer-associated genes. *Nature* 2013; **499:** 214–218.
29. Hofmann M, Stoss O, Shi D, *et al.* Assessment of a HER2 scoring system for gastric cancer: results from a validation study. *Histopathology* 2008; **52:** 797–805.
30. Dawood S, Hu R, Homes MD, *et al.* Defining breast cancer prognosis based on molecular phenotypes: results from a large cohort study. *Breast Cancer Res Treat* 2011; **126:** 185–192.
31. Alexandrov T, Chernyavsky I, Becker M, *et al.* Analysis and interpretation of imaging mass spectrometry data by clustering mass-to-charge images according to their spatial similarity. *Anal Chem* 2013; **85:** 11189–11195.
32. Yap TA, Gerlinger M, Futreal PA, *et al.* Intratumor heterogeneity: seeing the wood for the trees. *Sci Transl Med* 2012; **4:** 127ps110.
33. Aparicio S, Caldas C. The implications of clonal genome evolution for cancer medicine. *N Engl J Med* 2013; **368**(9): 842–851.
34. Bauer JA, Chakravarthy AB, Rosenbluth JM, *et al.* Identification of markers of taxane sensitivity using proteomic and genomic analyses of breast tumors from patients receiving neoadjuvant paclitaxel and radiation. *Clin Cancer Res* 2010; **16:** 681–690.
35. Hardesty WM, Kelley MC, Mi D, *et al.* Protein signatures for survival and recurrence in metastatic melanoma. *J Proteomics* 2011; **74:** 1002–1014.
36. Droin N, Hendra JB, Ducoroy P, *et al.* Human defensins as cancer biomarkers and antitumour molecules. *J Proteomics* 2009; **72:** 918–927.
37. Mohri Y, Mohri T, Wei W, *et al.* Identification of macrophage migration inhibitory factor and human neutrophil peptides 1–3 as potential biomarkers for gastric cancer. *Br J Cancer* 2009; **101:** 295–302.
38. Balluff B, Rauser S, Meding S, *et al.* MALDI imaging identifies prognostic seven-protein signature of novel tissue markers in intestinal-type gastric cancer. *Am J Pathol* 2011; **179:** 2720–2729.
39. Kim HK, Reyzer ML, Choi IJ, *et al.* Gastric cancer-specific protein profile identified using endoscopic biopsy samples via MALDI mass spectrometry. *J Proteome Res* 2010; **9:** 4123–4130.
40. Aichler M, Elsner M, Ludyga N, *et al.* Clinical response to chemotherapy in oesophageal adenocarcinoma patients is linked to defects in mitochondria. *J Pathol* 2013; **230:** 410–419.
41. Elsner M, Rauser S, Maier S, *et al.* MALDI imaging mass spectrometry reveals COX7A2, TAGLN2 and S100-A10 as novel prognostic markers in Barrett's adenocarcinoma. *J Proteomics* 2012; **75:** 4693–4704.
42. Dekker TJ, Balluff BD, Jones EA, *et al.* Multicenter matrix-assisted laser desorption/ionization mass spectrometry imaging (MALDI MSI) identifies proteomic differences in breast cancer-associated stroma. *J Proteome Res* 2014; DOI: 10.1021/pr500253j (in press).
43. Waanders LF, Chwalek K, Monetti M, *et al.* Quantitative proteomic analysis of single pancreatic islets. *Proc Natl Acad Sci USA* 2009; **106:** 18902–18907.

## SUPPLEMENTARY MATERIAL ON THE INTERNET

The following supplementary material may be found in the online version of this article:

**Protocol S1.** Assignment of *m/z* species of interest

**Protocol S2.** Optimization of the cluster presence threshold for comparison with clinical endpoints

**Figure S1.** Assessment of tumour diversity in breast cancer and clinical impact of each cluster across *k*.

**Figure S2.** Assessment of spectral similarities between subpopulations in two primary gastric cancers and their respective lymph node metastases.

**Figure S3.** Comparison of results if intra-tumor heterogeneity is not considered between our previous study and the current study on the identification of prognostic markers in gastric cancer.

**Figure S4.** Determination of the accurate mass of *m/z* 4156 by MALDI-FTICR high-resolution measurements.

**Figure S5.** Top-down fragmentation spectra of two *m/z* species of around 4151.35 (±0.7 Da) by both ETD and HCD.

**Table S1.** Multivariate survival analysis of components returned by agreement analysis on gastric cancer, using Cox regression model

**Table S2.** Top-down protein identification of tissue extracts

**Table S3.** Correlation of molecular subtypes in breast cancer with differences in heterogeneity or presence of a certain cluster (tumour subpopulation)